Photophysical Properties of Fluorescence Probes. 2. A Model of Multiple Fluorescence for Stilbazolium Dyes Studied by Global Analysis and Quantum Chemical Calculations†

Bernd Strehmel,* Holger Seifert, and Wolfgang Rettig

Institut für Physikalische und Theoretische Chemie, Humboldt-Universität zu Berlin, Bunsenstrasse 1, D-10117 Berlin, Germany

Received: September 13, 1996; In Final Form: December 10, 1996⊗

Photophysical properties of *o*-, *m*- and *p*-(dimethylamino)stilbazolium dyes were investigated using both time-resolved fluorescence spectroscopy and semiempirical quantum chemical calculations. The global analysis technique was applied to construct the spectral profiles of several emitting states. The results indicate that three exponential decays are necessary to globally describe the wavelength dependent fluorescence of the compounds investigated. The decay associated spectra obtained were taken to obtain kinetic information about the photophysical processes in the excited state. Two rise time components observed indicate that a consecutive reaction mechanism A → B → C dominates. The quantum chemical calculations indicate the presence of energetically low lying charge transfer states for twisted conformations. Both twist of the double bond and twist of the adjacent single bonds result in states comparable in energy to that of the planar conformation, while the twist of the dimethylamino group leads to an energetically higher lying twisted intramolecular charge transfer state, unlikely to be populated thermally. The state formed by twisting of the double bond possesses a remarkably low energy gap to the ground state, which causes mainly nonradiative deactivation. Both techniques together, global analysis and semiempirical calculations, show the validity of a model of multiple fluorescence for the compounds investigated.

Introduction

Substituted stilbazolium salts exhibit a very strong temperature effect on the fluorescence above the glass transition temperature of polymers and ordinary solvents[1−5] interpretable as dependence on the solvent surrounding.[4−6] In general, such a dependence offers many applications in different fields of science.[1,2] Some of these applications exist in medicine where these and related dyes are used as fluorescence indicators in neurons[7,8] because they exhibit a strong charge shift upon light excitation. This property can be used to detect differences in membrane potentials of biological materials. However, the strong viscosity dependence of the photophysical properties also offers several applications in polymer science and analytical chemistry.

The photophysics and photochemistry of 4-(dialkylamino)-4′-azastilbenes were investigated earlier with stationary fluorescence measurements, isomerization experiments, and pulse radiolysis.[5] An important property, the simultaneous dependence of photophysics on solvent viscosity and polarity, was found for stilbazolium and related (aminophenyl)pyridinium dyes by Fromherz et al.[4,9,10] These authors discuss the results by invoking single-bond twisting in the excited state toward a "twisted intramolecular charge transfer" (TICT) state[11−13] as the main cause for these dependencies. The validity of the TICT-model was approved by synthesis of a model compound[10] where the flexible single bond between the pyridinium and anilino group was bridged to obtain a rigid molecule (2-methyl-7-(dimethylamino)-2-azafluorenium). This substance possesses fluorescence quantum yields of about 50%. On the other hand, the efficiency for fluorescence of the twistable compound ((aminophenyl)pyridinium) is relatively low (0.05%) in solvents of high polarity and fluidity.[9,10]

On the basis of the results presented in a previous article,[14] we want to show here that the model of multiple fluorescence can reasonably well explain the photophysical properties of substituted (dialkylamino)stilbazolium salts. The goal of this work is to show that fitting the fluorescence decays at different wavelengths and the application of semiempirical quantum chemical calculations are able to explain the complex emission behavior of the compounds investigated in this work.

Previous studies have shown that the method of global analysis is a successful technique to characterize, for example, the dual emission behavior of excimers,[15,16] exciplexes,[17−20] and (dialkylamino)benzonitriles[21] or to analyze acid base equilibria of β-naphthol in the excited state.[22−25] These authors used different ways to obtain more detailed information about the emission properties of the compounds investigated. They focused on the evaluation of reaction rate constants, which was possible from the knowledge of the emission rate constants of the individual species involved.

An alternative way is to focus on the profiles of the fluorescing species, which was introduced by Löfroth.[26] This method has the advantage that the spectra of several simultaneously emitting states can be evaluated from the wavelength-resolved fluorescence decays even if no detailed information about the emission rates of the emitting species is known. It can easily be applied to systems where only one ground state species absorbs. Therefore, this method is useful for the characterization of wavelength dependent fluorescence decays with several overlapping fluorescence bands if characteristic rate constants of the emission behavior of the excited states are not available and if a separation of the individual states is not possible.

Semiempirical quantum chemical calculations are a complementary tool to characterize charge transfer states formed in photochemical processes. This method has been applied successfully to show that highly polar TICT states are energetically available through intramolecular twisting (for reviews, see refs

† Dedicated to Prof. Dr. H. G. O. Becker on the occasion of his 75th birthday.

* Corresponding author.

⊗ Abstract published in *Advance ACS Abstracts,* February 15, 1997.

S1089-5647(96)02835-0 CCC: $14.00

11−13) of molecular subgroups in different substituted stilbene derivatives.[13,14] This method can also show the direction and degree of electron transfer in the molecule. Within the limits of this method, we can explain the multiple fluorescence found experimentally for the compounds investigated in this work. The calculations show that both single bonds adjacent to the ethylenic group lead to low lying twisted intramolecular charge transfer states with possibly emissive properties. On the other hand, twisting of the double bond leads to an excited state considerably lower in energy than the planar one. Those states possess a nonemissive character because of the small energy gap between ground and excited state.[27] These results are used as a basis for the discussion and comparison of the results obtained by the global analysis technique. Results obtained by both global analysis and quantum chemical calculations will be compared to show the validity of the proposed model of multiple fluorescence.

Experimental Part

Materials. The dyes *p*-DASPMI and *o*-DASPMI and the solvent ethanol were purchased from Aldrich. The synthesis of *m*-DASPMI was described in a previous publication.[14] The purity of all compounds was checked by thin layer chromatography.

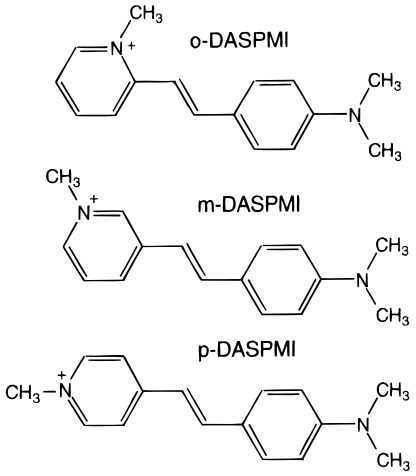

Stationary Fluorescence. Absorption spectra were measured with a UV-210 A from Shimadzu. Fluorescence spectra were recorded with a Perkin Elmer 650-60 fluorimeter using a correction curve determined with basic blue.[28] All emission spectra were measured with a spectral band-pass of 5 nm using 1 cm quartz cuvettes. The emission was detected in perpendicular geometry. Temperature dependent measurements were carried out with an equipment described earlier.[29]

Fluorescence Lifetimes. Fluorescence lifetime measurements were performed at the Berlin Electron Storage Ring for Synchrotron Radiation (BESSY) in the single-bunch mode (4.8 MHz repetition rate[29]) using single-photon-counting detection with iterative reconvolution.[30] By means of a monochromator (12.5 cm focal length, Jobin Yvon) the excitation wavelength was selected from the spectral continuum of the synchrotron radiation. Standard electronics from ORTEC was used for the time-correlated single-photon-counting technique, and the emission wavelength was selected using a similar monochromator (bandwidth 20 nm). A microchannel plate photomultiplier (Hamamatsu R1564-U-01) cooled to −25 °C was used for the detection. The channel width of the multichannel analyzer was 50 ps. Further details about the single-photon-counting equipment were described in a previous publication.[29] The global analysis of the decay curves at different wavelengths was carried out with a commercially available program.[31]

Quantum Chemical Calculations. Energy gaps between ground and excited states were calculated within the CNDO/S framework of DelBene and Jaffé[32,33] using the QCPE program #333 with the original parameters but modified to cope with larger molecules and to calculate excited-state dipole moments and charge distributions. Generally, configuration interaction (CI) between 40 and 50 singly excited configurations was used and compared to results from a CI calculation including additionally 45−90 doubly excited configurations. Ground state energies were calculated with the AM1 method contained in the program AMPAC 5.0 from SEMICHEM Inc. with the same geometries used for the CNDO/S calculations.

Standard geometries were used (bond lengths R(C−C) = 1.40 Å, R(C−H) = 1.083 Å, angles 120°) except for the ethylenic bond (R(C═C) = 1.33 Å) and the adjacent single bonds (R(C−C) = 1.45 Å, angle 128°[34,27]). The DASPMI isomers were generated from the stilbene skeleton by replacing hydrogens with the different substituents: dimethylamino ($R(C_{ar}-N)$ = 1.37 Å, $R(N-CH_3)$ = 1.46 Å, angles 120°, with tetrahedral CH_3 groups (R(C−H) = 1.083 Å)[34,35]). For the hetero ring in the DASPMI derivatives, the same regular hexagon was used, with the exocyclic methyl group at R(N−C) = 1.46 Å. The planar geometry assumed all dihedral angles as zero, and for the twisted isomers (φ = 90°), the remainder of the molecule was kept rigid. Molecular orbitals presented in this work were drawn with the program MOPLOT[36] from the output of the CNDO/S program.

Results and Discussion

Global Analysis in Ethanol. Steady state spectra measured at different temperatures and some photophysical properties of the different isomers for (dialkylamino)stilbazolium salts (*o*-DASPMI, *m*-DASPMI, *p*-DASPMI) were presented in a previous publication.[14] They are strongly dependent on both solvent viscosity and temperature but independent of concentration within the range investigated. Figure 1 shows the spectra for the three isomers recorded at 178 K in ethanol. As can be seen, the spectra are not structured. Furthermore, it was suggested[14] that a multiple photophysical mechanism is responsible for changes of the spectra at different temperatures/viscosities. In this article, we want to give a deeper insight into the mechanistic behavior using the fluorescence at lower temperatures/high viscosities in ethanol. For this reason, the dynamics of the fluorescence were studied in more detail with the global analysis technique.

The fluorescence decays were collected at different wavelengths for each compound. A typical example is given for some characteristic decay curves at different wavelengths in Figure 2. It can be seen that at short wavelengths (520 nm) at least two decay components are detectable. The weight of the short decay time decreases with increasing detection wavelength (see decay at 600 nm), and at least one rise component was observed in the red part of the emission spectrum. A global fit of the emission data for a given temperature showed that for all three isomers a three-exponential model was necessary in order to obtain an acceptable fit. An analysis with less than three exponents led to worse fit results, or the program did not show any convergence (Table 1).

The results fitted were used to construct the decay associated spectra (DAS) according to eq 1.[26] They are the normalized preexponential factors of the exponential functions that are used for the global fit analysis. The DAS values are wavelength dependent. They are the fit parameters at each wavelength λ

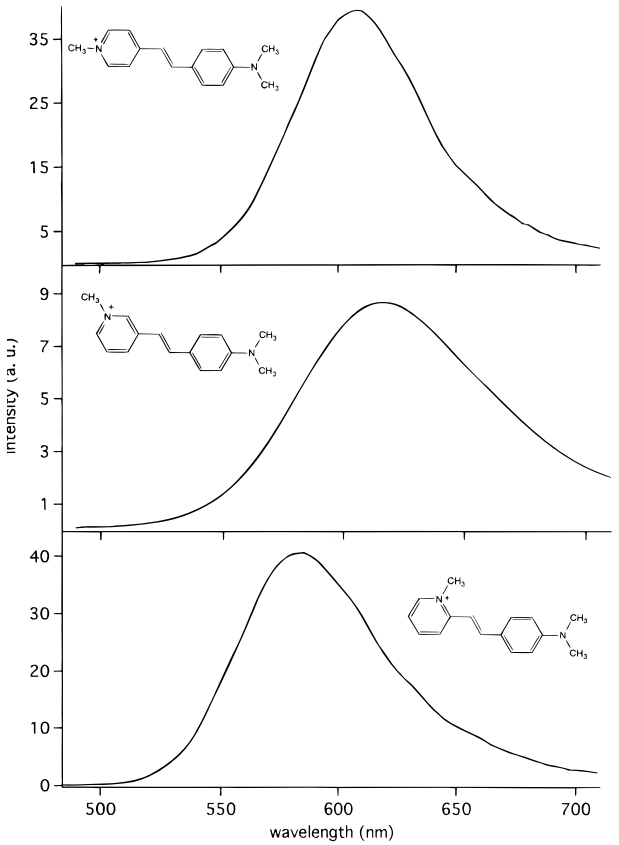

Figure 1. Steady state fluorescence spectra for *o*-, *m*- and *p*-DASPMI at 178 K in ethanol ($\lambda_{exc} = 470$ nm).

together with the decay times that are wavelength independent fit parameters.

$$\mathrm{DAS}(\lambda,\theta_i) = \frac{\alpha_i(\lambda)}{\sum_{j=1}^{n} \frac{\alpha_j(\lambda)}{\theta_j}} \mathrm{ISS}(\lambda) \qquad (1)$$

where α is the preexponential factor of the component i at the wavelength λ, θ is the inverse decay time of the component that was obtained in the global fit by linking of each decay time over the wavelengths, n is the number of exponents used for the fit in the global analysis, and ISS is the dimensionless relative intensity of the steady state spectrum at the wavelength λ.

The resulting DAS spectra for *p*-DASPMI are plotted in Figure 3. It can be seen from the negative DAS values that two rise components are present in the red part of the fluorescence spectrum. This behavior was observed for all three isomers, but the corresponding rise times ($\tau_f(1)$ and especially $\tau_f(2)$ in Table 1) are distinctly different. On the basis of the proposed model of multiple fluorescence, we want to show that DAS-spectra can be used to evaluate the reaction mechanism in the excited state and the profiles of the species associated spectra (SAS). This method is an alternative to a global target fit, which requires the knowledge of reference values (e.g. spectral shape of the emitting species, rate constants in the excited state). One can derive the following conclusions from the DAS data as compared to other common methods applied in global target fits:

(1) A rough estimate of excited state reaction mechanisms can be done because the signs of the DAS data can differ for different reaction mechanisms.

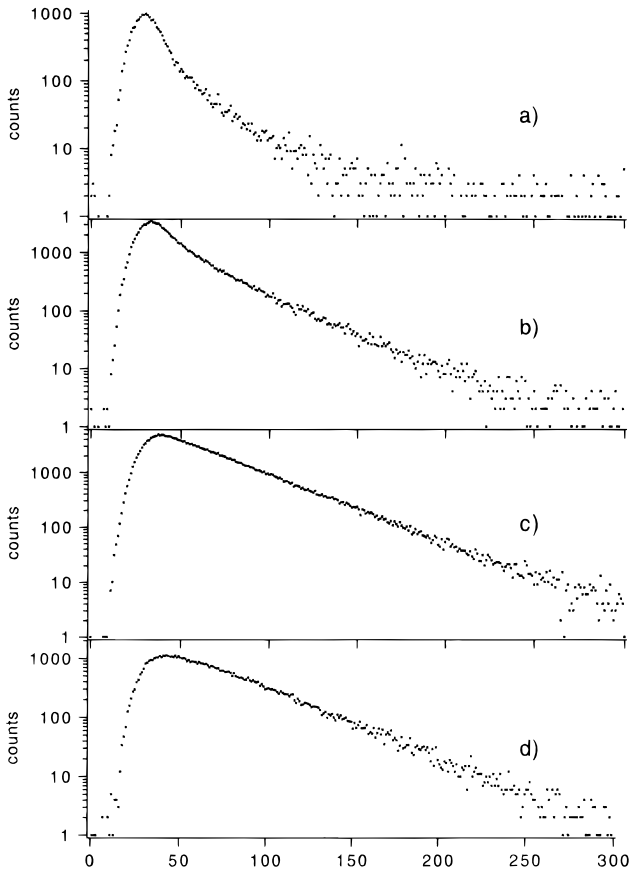

Figure 2. Fluorescence decays and globally fitted curves for *p*-DASPMI in ethanol (178 K) at different emission wavelengths: (a) 530, (b) 560, (c) 600, and (d) 640 nm; the corresponding lifetimes fitted are summarized in Table 1 ($\lambda_{exc} = 470$ nm).

TABLE 1: Results of the Global Analysis for the DASPMI Isomers in Ethanol at 178 K as a Function of the Emission Wavelength

global data	DASPMI isomer		
global χ^2	ortho	meta	para
monoexponential	no convergence	no convergence	no convergence
biexponential	4.70	no convergence	5.30
triexponential	1.07	1.22	1.16
	fluorescence lifetimes for triexponential fit		
$\tau_f(1)$/ns	0.16	0.10	0.13
$\tau_f(2)$/ns	1.08	0.37	0.75
$\tau_f(3)$/ns	2.33	0.96	1.71

(2) The construction of the profiles for the SAS spectra from the DAS data is a preferable alternative to global target fits if no further information is known about the rate constants of the products formed in the excited state.

(3) Quenching is an often applied technique for evaluating the rate constants of the photochemical processes.[17−20,37] However, we cannot apply this method because we do not have a detailed knowledge about useful quencher molecules (complex formation in the ground state, reaction mechanism).

(4) Some other authors isolated the spectra of several emitting states by the addition of bases or acids. Under these circumstances it was possible to get information about the emission properties of only one emitting species. This procedure works sufficiently well in the study of acid−base equilibria, for example, of β-naphthol,[24,25] where the two different species can be isolated and investigated separately. However, this procedure is excluded here because protonated DASPMI is a different chromophore.

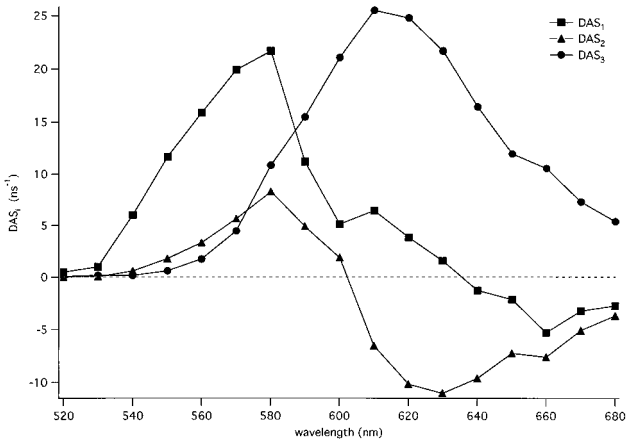

Figure 3. DAS spectra (relative values) for *p*-DASPMI in ethanol at 178 K, referring to the lifetimes in Table 1.

SCHEME 1: Generalized Kinetic Scheme for the Photophysical Processes of the DASPMI Isomers According to a Consecutive and Parallel Reaction Scheme Involving Three Excited Species A, B, C[a]

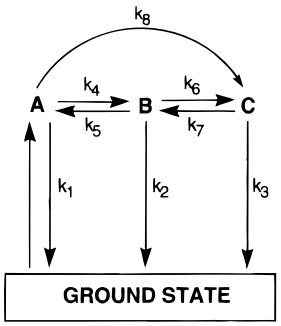

[a] After excitation, the relaxed Franck−Condon state A is reached. A can emit (k_1), or it can form new products B (k_4) and C (k_8), respectively. B can also show an emission (k_2), or it can also form C (k_6), which can also emit (k_3). Furthermore, each product B as well as C has in general the possibility for a back-reaction k_5 and k_7, respectively.

On the basis of the above results and the fluorescence behavior of DASPMI described earlier,[14] we propose the following kinetic model (see Scheme 1). This reaction scheme is similar to that suggested in the previous paper.[14] The results obtained by the investigation of (aminophenyl)pyridinium[9,10] underline the validity of this assumption. This compound possesses the same substructures (pyridinum, aminobenzene) in comparison to *p*-DASPMI, but it has only one flexible single bond that can contribute to a twisted intramolecular charge transfer. The introduction of a further double bond extends the possibility of twisted conformers (one double bond and two single bonds can twist) in one side, but the nature of the donor and the acceptor is approximately the same in both (aminophenyl)pyridinium and *p*-DASPMI. Therefore, the reaction mechanism proposed in Scheme 1 describes possible reactions in the excited state that are caused by an intramolecular charge transfer and the different possibilities to form twisted conformers. Furthermore, it should be remarked that all deactivation pathways described by the rate constants k_1, k_2, and k_3 to the ground state of DASPMI contain both emissive and nonradiative channels.

The next step is to set up the differential equations for the time dependent population of species A, B, and C on the basis of scheme I. However, a complete solution including all reactions proposed in this scheme would lead to very complicated mathematical expressions with solutions involving complex numbers. Therefore, we want to make some simplifying assumptions, which result in several simpler but mathematically treatable reaction schemes. We will show that these assumptions are justified within the limits of the model proposed by comparing the experimental data with the theoretical treatment of these simple schemes.

(a) Parallel Reaction Mechanism ($C \leftarrow A \rightarrow B$; $k_5 = 0$, $k_6 = 0$, $k_7 = 0$). The solution of the differential equation system was used to derive the following mathematical expressions for the DAS values (eqs 2−4) for the parallel reaction mechanism.

$$\mathrm{DAS}_1(\lambda) = (A_0 a(\lambda)) - \frac{k_4 A_0}{\theta_1 - \theta_2} b(\lambda) - \frac{k_8 A_0}{\theta_1 - \theta_3} c(\lambda) \quad (2)$$

$$\mathrm{DAS}_2(\lambda) = \frac{k_4 A_0}{\theta_1 - \theta_2} b(\lambda) \quad (3)$$

$$\mathrm{DAS}_3(\lambda) = \frac{k_8 A_0}{\theta_1 - \theta_3} c(\lambda) \quad (4)$$

(assumption: $\theta_1 > \theta_2, \theta_3$)

In this equation system, $a(\lambda)$, $b(\lambda)$, $c(\lambda)$ are the wavelength dependent spectral contours for the species A, B, and C and θ_1, θ_2 and θ_3 are reciprocal values of the globally fitted fluorescence decays. The spectral profiles $a(\lambda)$, $b(\lambda)$, and $c(\lambda)$ for the emitting species A, B, and C are defined by eq 5. Further mathematical details concerning the calculation of the spectral profiles $a(\lambda)$, $b(\lambda)$, and $c(\lambda)$ from both DAS and SAS are given in the Appendix.

$$\int_\lambda x(\lambda')\, \mathrm{d}\lambda' = k_\mathrm{f}^{\mathrm{X}} \quad (5)$$

where $x(\lambda')$ stands for the spectral contours $a(\lambda)$, $b(\lambda)$, and $c(\lambda)$ of the species A, B, and C, respectively. Integration of the spectral profiles yields the fluorescence rate constant k_f of the different species A, B, and C ($k_\mathrm{f}^{\mathrm{A}}$, $k_\mathrm{f}^{\mathrm{B}}$, $k_\mathrm{f}^{\mathrm{C}}$).

The expressions of the DAS values in the eqs 2−4 shows that only DAS_1 can become negative through the coefficients of $b(\lambda)$ and $c(\lambda)$. This demonstrates that in the case of a parallel reaction mechanism only one rise component is possible in the DAS spectra. However, we reported above that two rise components were observed for all three DASPMI isomers. As a result, we conclude that the parallel mechanism does not yield a proper description of our compounds. This result is underlined by the following considerations. The species associated spectra (SAS), which are the spectra of the emitting species A, B, and C, can be calculated from the solution of the differential equation system (see Appendix). A typical example is written in eqs 6−8 for the parallel reaction mechanism.

$$\mathrm{SAS}_\mathrm{A} = \frac{\mathrm{DAS}_1(\lambda) + \mathrm{DAS}_2(\lambda) + \mathrm{DAS}_3(\lambda)}{\theta_1} \quad (6)$$

$$\mathrm{SAS}_\mathrm{B} = \frac{(\theta_1 - \theta_2)}{\theta_1 \theta_2} \mathrm{DAS}_2(\lambda) \quad (7)$$

$$\mathrm{SAS}_\mathrm{C} = \frac{(\theta_1 - \theta_3)}{\theta_1 \theta_3} \mathrm{DAS}_3(\lambda) \quad (8)$$

(assumption: $\theta_1 > \theta_2, \theta_3$)

As can be seen, one can derive analytical expressions for SAS_A, SAS_B, and SAS_C, which do not contain any kinetic rate constants for the formation of B or C. We used this model equations for

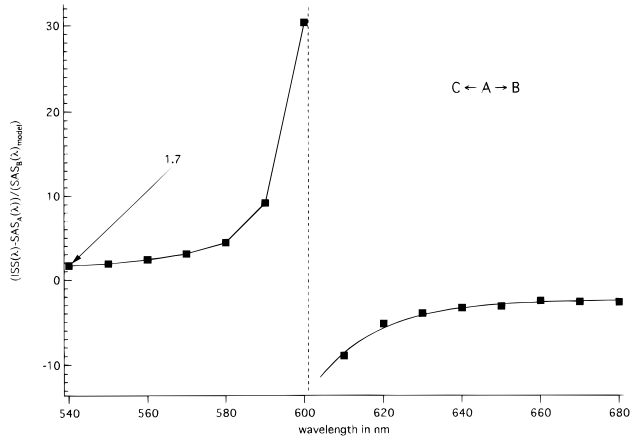

Figure 4. Model check for the parallel reaction mechanism ($k_5 = 0$, $k_7 = 0$, $k_6 = 0$) by extrapolation into the blue part of the emission spectrum according to eq 10 yielding a value significantly larger than 1.

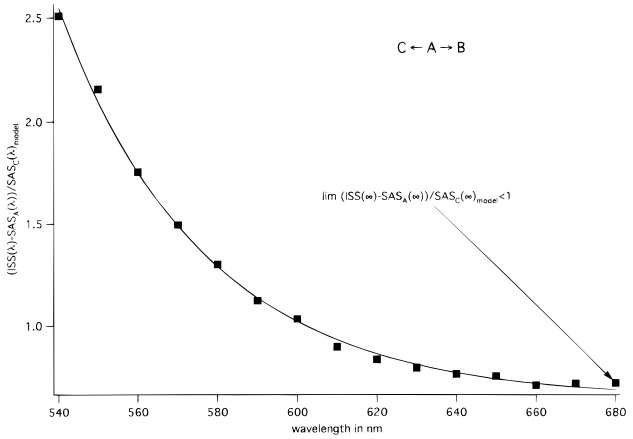

Figure 5. Model check for a parallel reaction mechanism ($k_5 = 0$, $k_7 = 0$, $k_6 = 0$) by extrapolation into the red part of the emission spectrum according to eq 9. A value significantly smaller than 1 is recovered.

a further check on whether the parallel mechanism assumed could be valid under our experimental conditions. Firstly, we subtracted the spectral profile for SAS_A from the intensity of the steady state spectrum ISS ($ISS(\lambda) - SAS_A(\lambda)$). This difference represents the sum of the experimental spectra $SAS_B + SAS_C$. Then, we calculated the model SAS for B and C according to the expressions in eqs 7 and 8. A division of ($ISS(\lambda) - SAS_A(\lambda)$) by SAS_B(model) and SAS_C(model), respectively, allows a decision about the validity of the model assumed by extrapolation into the blue ($\lambda \rightarrow 0$) as well as into the red ($\lambda \rightarrow \infty$) part of the spectrum; compare eqs 9 and 10. If these equations are fulfilled (the corresponding ratios converge toward 1 in the red and blue part of the spectrum, respectively), then the assumed model describes the experimental data sufficiently well. On the other hand, another model has to be checked.

$$\lim_{\lambda_{red}\rightarrow\infty} \frac{ISS(\lambda) - SAS_A(\lambda)}{SAS_C(\lambda)_{model}} = \frac{SAS_C(\lambda)_{exptl}}{SAS_C(\lambda)_{model}} = 1 \qquad (9)$$

$$(B_0 = C_0 = 0)$$

$$\lim_{\lambda_{blue}\rightarrow\infty} \frac{ISS(\lambda) - SAS_A(\lambda)}{SAS_B(\lambda)_{model}} = \frac{SAS_B(\lambda)_{exptl}}{SAS_B(\lambda)_{model}} = 1 \qquad (10)$$

$$(B_0 = C_0 = 0)$$

Equations 9 and 10 hold under the assumption that SAS_B and SAS_C differ and SAS_C is red shifted with respect to SAS_B with vanishing ground state populations of the products B and C. The results obtained for such an assumed parallel mechanism are plotted in the Figures 4 and 5. The limiting values according to eqs 9 and 10 do not converge to unity for $(ISS(\lambda) - SAS_A(\lambda))/SAS_C(\lambda)_{model}$ in the red part (compare Figure 5) and for $(ISS(\lambda) - SAS_A(\lambda))/SAS_B(\lambda)_{model}$ in the blue part of the emission spectrum (compare Figure 4), respectively. Especially the limiting value of $(ISS(\lambda) - SAS_A(\lambda))/SAS_C(\lambda)_{model} < 1$ in the red part of Figure 5 underlines that a parallel reaction mechanism does not describe the data under the experimental conditions used. Similar results are obtained for all three isomers investigated.

(b) Consecutive Reaction Mechanism ($A \rightarrow B \rightarrow C$; $k_5 = 0$, $k_8 = 0$, $k_7 = 0$). The solution of the differential equation system for this reaction mechanism (see Scheme 1) leads to the set of eqs 11−13 for DAS

$$DAS_1(\lambda) = A_0\, a(\lambda) - \frac{A_0 k_4}{(\theta_1 - \theta_2)} b(\lambda) + \frac{A_0 k_4 k_6}{(\theta_1 - \theta_3)(\theta_1 - \theta_2)} c(\lambda) \qquad (11)$$

$$DAS_2(\lambda) = + \frac{A_0 k_4}{(\theta_1 - \theta_2)} b(\lambda) - \frac{A_0 k_4 k_6}{(\theta_2 - \theta_3)(\theta_1 - \theta_2)} c(\lambda) \qquad (12)$$

$$DAS_3(\lambda) = + \frac{A_0 k_4 k_6}{(\theta_1 - \theta_3)(\theta_2 - \theta_3)} c(\lambda) \qquad (13)$$

and eqs 14−16 for SAS

$$SAS_A = \frac{DAS_1(\lambda) + DAS_2(\lambda) + DAS_3(\lambda)}{\theta_1} \qquad (14)$$

$$SAS_B = \frac{(\theta_1 - \theta_2)DAS_2(\lambda) + (\theta_1 - \theta_3)DAS_3(\lambda)}{\theta_1 \theta_2} \qquad (15)$$

$$SAS_C = \frac{(\theta_1 - \theta_3)(\theta_2 - \theta_3)}{\theta_1 \theta_2 \theta_3} DAS_3(\lambda) \qquad (16)$$

As can be seen from eqs 11−13, DAS_1 and DAS_2 can become negative in the case of the assumed consecutive reaction mechanism. The DAS values plotted in Figure 3 demonstrate that this mechanism could be valid within the error limits because both DAS_1 and DAS_2 have negative values in the red part of the fluorescence spectrum. Furthermore, the eqs 9 and 10 were also applied to check the validity of this model. SAS_A has the same expression for both mechanisms. Thus, the $(SAS_B)_{model}$ and $(SAS_C)_{model}$ were substituted with the analytical expressions SAS_B and SAS_C from eqs 14−16. The results obtained are plotted in Figure 6.

As can be seen from this plot, the limiting values approach a number that is close to 1 for $(ISS(\lambda) - SAS_A(\lambda))/(SAS_B)_{model}$ in the blue part and $(ISS(\lambda) - SAS_A(\lambda))/(SAS_C)_{model}$ in the red part (Figure 6). This result supports the assumption that a consecutive mechanism with $k_5 = 0$, $k_8 = 0$, $k_7 = 0$ dominates under the experimental conditions used.

(c) Consecutive Reaction Mechanism with One Back-Reaction ($A \rightarrow B \rightleftarrows C$; $k_5 = 0$, $k_8 = 0$, $k_7 \neq 0$). In a further treatment, we can show the validity of the assumption that $k_7 \approx 0$ for the consecutive reaction mechanism. For this reason, the rate constant k_C is introduced, which is the sum of all deactivating

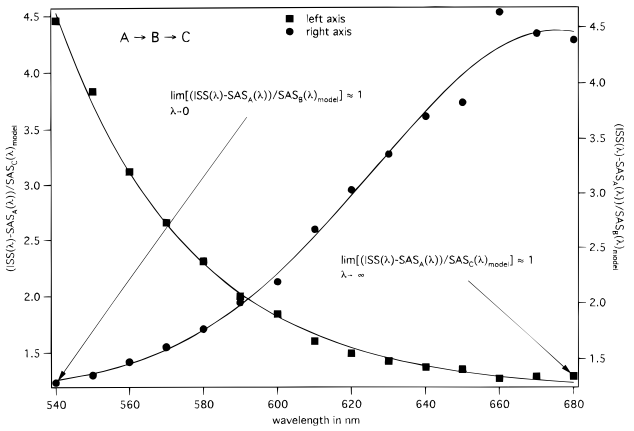

Figure 6. Model check for a consecutive reaction mechanism ($k_5 = 0$, $k_7 = 0$, $k_8 = 0$) by extrapolation into the red part of the emission spectrum according to eq 5 and extrapolation into the blue part of the emission spectrum according to eq 6, respectively.

processes for species C including the rate constant k_7 for the back-reaction. In the case that $k_7 \approx 0$, one can see in eq 17

$$k_C = k_3 + k_7 \tag{17}$$

that k_C is equal to the inverse fluorescence lifetime θ_3 ($\theta_3 = k_C = k_3$). Löfroth[26] proposed a procedure for the determination of k_C. The solution of the differential equations for this reaction mechanism with $k_7 \neq 0$ leads to the following equations for SAS_B and SAS_C. SAS_A can be easily calculated in the same way as described above because it has the same analytical expression.

$$SAS_B(\lambda) = \frac{(\theta_1 - \theta_2)DAS_2(\lambda) + (\theta_1 - \theta_3)DAS_3(\lambda)}{\theta_1\theta_2\theta_3}k_C \tag{18}$$

$$SAS_C(\lambda) = \frac{(\theta_1 - \theta_3)(\theta_2 - k_C)DAS_3(\lambda) - (\theta_1 - \theta_2)(k_C - \theta_3)DAS_2(\lambda)}{\theta_1\theta_2\theta_3}k_C \tag{19}$$

By replacing $SAS_B(\lambda)$ in eq 18 with $ISS(\lambda) - SAS_A(\lambda)$ (assuming that the spectral overlap of B and C can be neglected in the blue part of the emission spectrum and only species B is emitting there), eq 20 is obtained for k_c, which can be called an apparent function because k_c is expected to converge to its true value only in the blue part of the spectrum where the spectral contribution of C can be neglected. In general, this procedure is similar to that described above regarding eqs 9 and 10.

$$\lim_{(\lambda\to 0)} (k_C^{app}(\lambda)) = \frac{(ISS(\lambda) - SAS_A(\lambda))\theta_1\theta_2\theta_3}{(\theta_1 - \theta_2)DAS_2(\lambda) + (\theta_1 - \theta_3)DAS_3(\lambda)} \tag{20}$$

$k_C^{app}(\lambda)$ can be determined by plotting the right-hand side of eq 20 versus the wavelength and extrapolating into the blue part. The results obtained for *p*-DASPMI according to eq 20 are drawn in Figure 7. A slight plateau with an extrapolated value $k_c \approx 0.7$ ns^{-1} (error $\approx \pm 15\%$) is reached in the blue region of the emission spectrum. It possesses nearly the same value as the inverse fluorescence lifetime $\theta_3 = 0.58$ ns^{-1} (compare Table 1). Similar results ($k_c \approx \theta_3$) were also obtained for the other DASPMI isomers. As a result from these data we can conclude that the back-reaction can be neglected ($k_7 \ll k_3$) for all three isomers because eq 17 can be reduced to $k_C \approx k_3 \approx \theta_3$. On the other hand, a careful view of the data in Figure 7 leads to the conclusion that extrapolation into the blue part is

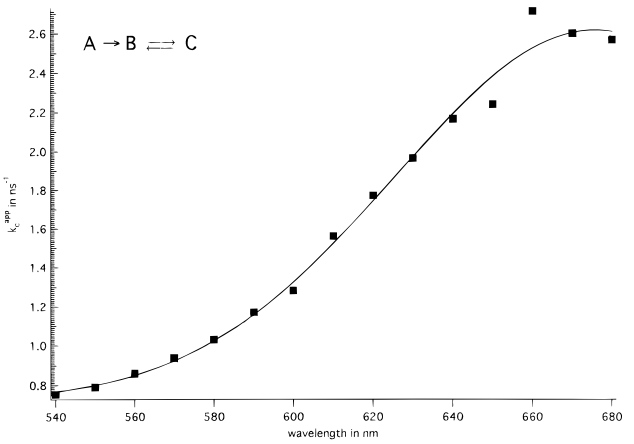

Figure 7. Determination of k_C^{app} by extrapolation using eq 20 versus wavelength for *p*-DASPMI in ethanol at 178 K.

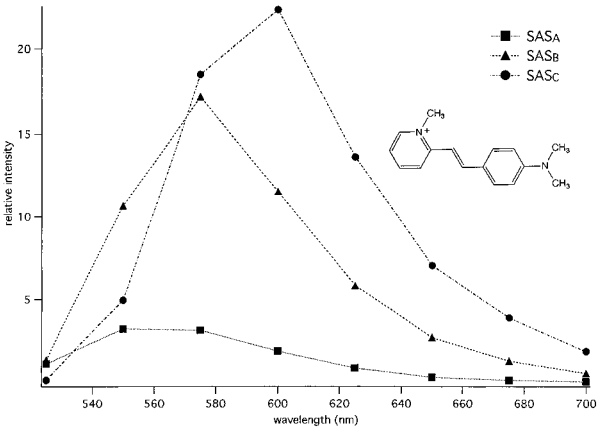

Figure 8. SAS spectra for *o*-DASPMI at 178 K in ethanol according to a consecutive reaction mechanism.

difficult if the spectra of species B and C do overlap. Therefore, this procedure allows only a rough estimate about the validity of this reaction mechanism. However, it is an alternative to the global target fit[25] needing additional data.

With the assumption of the kinetic scheme applicable to our system, the profiles for SAS_A, SAS_B, and SAS_C were constructed in the next step. The above discussion supports the consecutive mechanism with $k_7 \approx 0$ (case b) as appropriate to describe the emission behavior of all three DASPMI isomers satisfactorily for the experimental conditions used. The resulting SAS are drawn in Figures 8−10. It can be seen that the relative weight of SAS_A is small for all three isomers while SAS_B and SAS_C constitute the main contributions to the emission spectrum. This result confirms the multiple nature of fluorescence. This multiple fluorescence can in principle be due to

(i) the relaxation of the surrounding solvent toward solvated species or

(ii) to the inter- or intramolecular relaxation of the solute.

As the observed rise times are distinctly different for the three isomers (Table 1), we may exclude possibility i because the relaxing solvent is equal in all three cases. On the basis of the concentration independence observed, we can also exclude a bimolecular solute−solute mechanism, and we believe that a monomolecular solute relaxation mechanism occurs as the most likely interpretation of the kinetic results observed. In the following part we present arguments that the well-known model of twisted intramolecular charge transfer states (TICT)[11−13] can serve as a good basis to explain the multiple fluorescence of the DASPMI isomers.

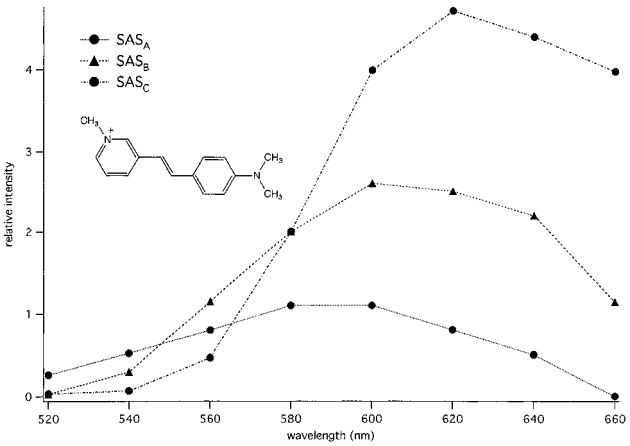

Figure 9. SAS spectra for *m*-DASPMI at 178 K in ethanol according to a consecutive reaction mechanism.

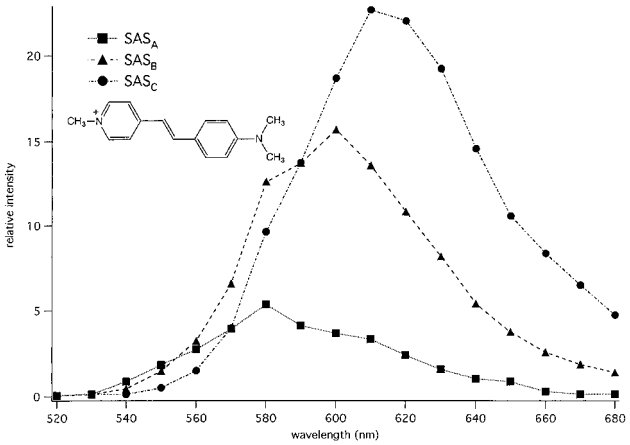

Figure 10. SAS spectra for *p*-DASPMI at 178 K in ethanol according to a consecutive reaction mechanism.

According to this model and owing to the possibility of twisting around several different single bonds similarly to the donor acceptor stilbenes[38−41] as well as around the double bond, the following photoreaction steps starting from the initially reached excited state E* with planar conformation can be envisaged to occur in the excited state. Moreover, twisting of the anilino group was also shown in (aminophenyl)pyridinium that has a similar structure in comparison to the compounds investigated in this work.[9,10] Bridging of the flexible single bond between the pyridinium and the anilino group leads to a tremendous increase of the fluorescence quantum yield.[9,10] The results obtained with these compounds were discussed with a two-state model in the excited state.

(1) Twisting of the olefinic double bond toward an angle of 90°: The deactivation of the relaxed twisted species P* should occur mainly by radiationless processes because the energy gap between excited and ground state is very small[27] (see also below for more detailed quantum chemical results). This nonradiative deactivation by double-bond twisting is supposed to gain importance at lower viscosities because of the larger reaction volume for this movement as opposed to the single-bond twisting pathway.[14]

(2) Twisting of one or both single bonds neighboring the olefinic double bond according to the TICT mechanism: in this case the deactivation of the excited state with single-bond twisted geometry can also occur by fluorescence because the S_0-S_1 gap is larger. This idea agrees well with data published about the photochemistry of (aminophenyl)pyridinium.[9,10] The results obtained were compared with a rigid model compound.

SCHEME 2: Several Possibilities of Twisted Conformations in the Case of *p*-DASPMI[a]

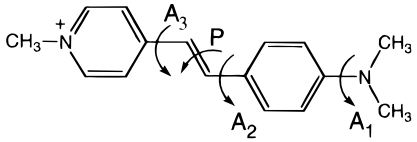

[a] The Label A stands for the twist of a single bond with the index denoting the position, and P corresponds to the twist of a double bond. E denotes the planar system.

They led to the conclusion that twisting of the phenyl group is the dominant process in the excited state.[9,10]

(3) Twisting of the dimethylamino group: This process can be neglected, because according to calculation results the corresponding CT state formed possesses an energy which is more than 1.5 eV higher in comparison with the planar conformation (E*).

In the following, quantum chemical calculations are applied to study some spectroscopic properties of the states that can be formed in the reaction mechanism postulated.

Quantum Chemical Investigations. Excited-state energy calculations were carried out for the various twisted conformations, with a twist angle of 90° for the twisted bond to characterize the limiting TICT conformations. Although the TICT states can be characterized by rather broad angular distributions,[13,38] the dipole moment or the charge localization for ionic systems always reaches a maximum for this limiting conformation with perpendicular and thus decoupled π-orbitals.[13,38−40] All singly twisted conformations were investigated, with the twisted double bond (conformation P), the two single bonds of the styryl group (conformations A_2, A_3), and the single bond between the dimethylamino group and the phenyl group (A_1). The labels indicate which of the single bonds is twisted; see also Scheme 2.

The results obtained by the CNDO/S calculations can give a rough guideline regarding the energies of possible excited product states. However, as only the difference between the ground and the excited states is calculated with this method, the energies have to be corrected by the increase of the ground state energy. This holds especially for twisting the double bond (see results below). On the other hand, the ground state influence is negligible (≈0.1 eV) if only single-bond twisted species are compared (see also the discussion below). In view of the qualitative nature of the calculations, the influence of polar solvents was not taken into account. However, a general trend of polar solvents will be to stabilize the charge-separated or charge-localized states of the twisted conformations more strongly than the excited states of the planar conformations due to the maximization of charge separation.[13] These results are useful for comparisons: they allow to pinpoint those twisted single bonds that lead to especially low lying TICT states. If the energy of these TICT states is below or within thermal reach of the energy of the initial state E, they might be expected to be populated and to contribute to the emission spectrum observed.

The following properties can be used to define the TICT states in the DASPMI compounds investigated:

the positive charge is nearly fully localized in one of the twisted parts;

the calculated transition moment is close to zero for the limiting perpendicular conformation;

as compared to the twisted ground state, the positive charge is translocated from one molecular part to the other one of the twisted molecule; The excited-state energies for the different twisted conformations as calculated for the three DASPMI

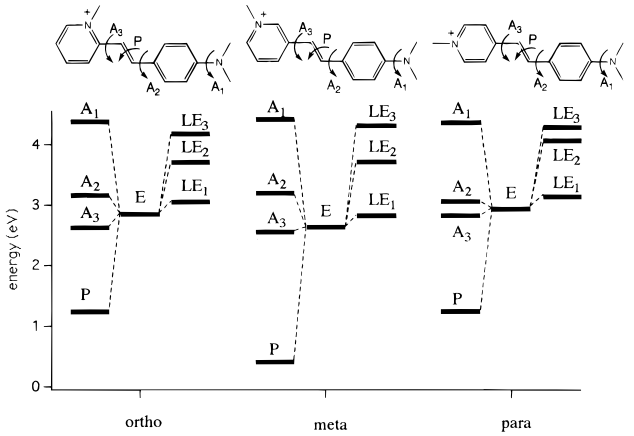

Figure 11. Calculated energy gaps between S_0 and the lowest excited states for several conformations of the DASPMI isomers. The index 1, 2, or 3 identifies the twisted single bond, while P corresponds to the twisted double bond. LE are the lowest locally excited states and A are the lowest TICT states for a given single-bond twisted conformation, while E is the lowest excited state for the planar conformation.

isomers are plotted in Figure 11. The index 1, 2, or 3 relates to the numbering of twisted single bonds, while P corresponds to the twisted double bond; see Scheme 2. The letter A in this figure is used to denote the lowest TICT states, while LE are the lowest locally excited states of the twisted systems where the electronic excitation resides in one of the moieties. The LE states possess large transition moments, while that of the A states is close to zero. E denotes the lowest excited singlet state of the planar system.

Figure 11 shows that twisting of the dimethylamino group (index 1) leads to a TICT state (A_1) that is considerably higher in energy than the nontwisted conformation E. On the other hand, rotation around one of the single bonds of the olefinic styryl group (index 2 or 3, see Scheme 2) leads to TICT states with an energy close to that of E. A simultaneous fluorescence from E, A_2, and/or A_3 is therefore a likely explanation for the broad steady state spectra measured[14] and for the multiple fluorescence observed by the global analysis in this work. Furthermore, twisting of the double bond (P state) leads to a rather close approach of S_1 and S_0 which may be connected with a large ground state barrier. *m*-DASPMI possesses the smallest S_0-S_1 energy gap for the P state, while in the case of the ortho and para-derivatives somewhat larger but nearly equal energy gaps were calculated.

For a discussion of the quantum chemical results, calculations were also performed which included doubly excited configurations in order to study their importance for the excited states calculated. The inclusion of interaction with doubly excited configurations (DCI) is only a step in the direction toward full CI which would be preferable. As an example for the effect of DCI, Table 2 collects the results for the four lowest excited singlet states for the different twisted conformations of *p*-DASPMI. It can be seen that doubly excited configurations only marginally contribute to all the states reported except for a few cases, for higher lying states like the S_3 or S_4 states, where a weight of doubly excited configurations of up to 15% was calculated. The results are interesting especially for the discussion of the lowest excited state S_1 of the double-bond twisted conformation P, because this state is often discussed in the literature (e.g. stilbenes) as represented by a "doubly excited" state.[42] In the present molecules, these states seem to be much higher lying, and the lowest excited state for the conformation P is better described as a biradicaloid state.[27,43] The large value for the ground state energy depression only for conformation P

TABLE 2: Effect of Doubly Excited Configurations for *p*-DASPMI

conformation[a]	state[b]	E(SCI)[c] (eV)	*E*(DCI)[d] (eV)	%*D*[e]	ground state energy depression[f]
E	S_1	2.92	2.68	4.6	−0.11
	S_2	4.11	3.93	5.0	
	S_3	4.32	4.10	4.6	
	S_4	4.71	4.42	12.5	
A_1	S_1	3.12	3.04	2.0	+0.077
	S_2	4.11	3.95	3.2	
	S_3	4.35	4.16	2.3	
	S_4	4.47	4.41	3.2	
A_2	S_1	3.04	2.96	2.0	−0.13
	S_2	4.04	3.91	3.2	
	S_3	4.27	4.17	2.3	
	S_4	4.58	4.48	6.9	
A_3	S_1	2.44	2.48	1.5	−0.13
	S_2	3.79	3.82	1.5	
	S_3	4.29	4.08	5.9	
	S_4	4.31	4.35	<1	
P	S_1	1.23	1.7	<1	−0.53
	S_2	3.61	3.58	3.58	
	S_3	3.72	4.06	14.8	
	S_4	4.2	4.25	1.2	

[a] Determines the kind of twisting; see Scheme 2. [b] Singlet states. [c] Energies using CI singly excited configurations only. [d] Energies using DCI. [e] Relative contribution of doubly excited configurations. [f] Effect of DCI inclusion.

indicates that, contrary to S_1, the ground state considerably mixes with doubly excited configurations.

Table 3 contrasts the results for ortho, meta, and para-isomers for the different twisted conformations and also gives a state assignment based on orbital analysis which allows location of the TICT states for the various conformers. For the nontwisted conformation E, a strong intramolecular charge transfer was found for all three isomers similar to the results described for *p*-DASPMI by Fromherz.[4] If the dimethylamino group is twisted by 90° (A_1 conformation), the lowest TICT state is S_4 in the case of the ortho and meta-compound and S_3 for the para-isomer. Its energy is estimated to be too large for a thermal population from E. The lower states are locally excited states without charge migration from one moiety to the other upon excitation. For the A_2 and A_3 conformations, the lowest TICT state is situated much lower in energy (S_1 in all cases with an additional TICT state as S_2 and S_3 depending on the isomer).

Further insight can be gained by a closer look at the molecular orbitals. This also allows to draw a comparison to stilbene. For all isomers in the nontwisted conformation, S_1 consists mainly of the HOMO−LUMO transition, and therefore only the frontier orbitals need to be considered. In Figure 12 the HOMO and LUMO for the three isomers of DASPMI are plotted. In contrast to stilbene,[27] which possesses coefficients on both carbon atoms of the double bond, the coefficients in the case of the DASPMI isomers are alternating in the HOMO and in the LUMO. This property is typical for cyanine dyes and underlines that the stilbazolium dyes investigated can be described as disturbed cyanines..[27] Another difference from stilbene is the nearly complete lack of photoisomerization: the stilbazolium compounds do not efficiently isomerize in alcohols, and they do also not bleach during irradiation in the absorption band.[5] The reason for this phenomenon may exist in another pathway for the twist of the double bond that is different in comparison to the reaction path for the trans → cis photoisomerization for common substituted stilbenes. These effects lead us to the conclusion that DASPMI and stilbene are quite different classes of compounds although a theoretical bridge with the biradicaloid model[13,27,43] connects them.

TABLE 3: Calculated Excitation Energies, Oscillator Strength *f*, and State Characterization (char.) for the DASPMI Isomers

conf[a]		*o*-DASPMI				*m*-DASPMI				*p*-DASPMI			
E	state[b]	S1	S2	S3	S4	S1	S2	S3	S4	S1	S2	S3	S4
	E (eV)[c]	2.85	4.1	4.13	4.45	2.63	3.32	4.16	4.34	2.92	4.11	4.32	4.71
	f[e]	0.55	0.091	0.001	0.021	0.071	0.49	0.0063	0.091	0.6	9.7E−4	1.1E−4	0.029
	char.	ICT	ICT	ICT	ICT	ICT	LE	ICT	ICT	ICT	ICT	ICT	LE
A1	state[b]	S1	S2	S3	S4	S1	S2	S3	S4	S1	S2	S3	S4
	E (eV)[c]	3.04	4.14	4.35	4.37	2.81	3.54	4.3	4.4	3.12	4.11	4.35	4.47
	f[e]	0.52	0.0055	0.0096	9.6E−5	0.075	0.46	1.5E−3	1.1E−5	0.59	5.0E−3	3.4E−5	0.002
	char.	LE	LE	LE	TICT	LE	LE	LE	TICT	LE	LE	TICT	LE
A2	state[b]	S1	S2	S3	S4	S1	S2	S3	S4	S1	S2	S3	S4
	E (eV)[c]	3.15	3.71	4.37	4.38	3.18	3.35	3.71	4.23	3.04	4.04	4.27	4.38
	f[e]	5E−6	0.4	6.3E−4	0.021	2E−6	0.094	6.1E−5	0.035	2E−6	0.51	9.3E−3	0.021
	char.	TICT	LE	TICT	LE	TICT	TICT	LE	LE	TICT	LE	TICT	LE
A3	state[b]	S1	S2	S3	S4	S1	S2	S3	S4	S1	S2	S3	S4
	E (eV)[c]	2.62	3.94	4.18	4.3	2.54	3.71	4.29	4.3	2.91	4.04	4.27	4.38
	f[e]	2E−6	1.6E−3	0.58	1.9E−2	9E−5	1.0E−5	0.37	0.029	1E−5	1.7E−4	0.06	$<10^{-6}$
	char.	TICT	TICT	LE	LE	TICT	TICT	LE	LE	TICT	TICT	LE	TICT
P	state[b]	S1	S2	S3	S4	S1	S2	S3	S4	S1	S2	S3	S4
	E (eV)[c]	1.23	3.24	3.94	4.2	0.41	1.69	3.28	3.89	1.23	3.61	3.72	4.2
	f[e]	8E−6	0.31	0.29	0.029	1E−5	0.041	0.42	0.0026	6E−6	0.47	0.14	0.043
	char.	BR[d]	LE	LE	LE	BR[d]	LE	LE	LE	BR[d]	LE	LE	LE

[a] Determines the kind of twisting (see Scheme 2). [b] Singlet states. [c] Energy gaps to the ground state. [d] Biradicaloid state with excitation between the frontier orbitals of the subchromophores. [e] Read as for example 5×10^{-6}.

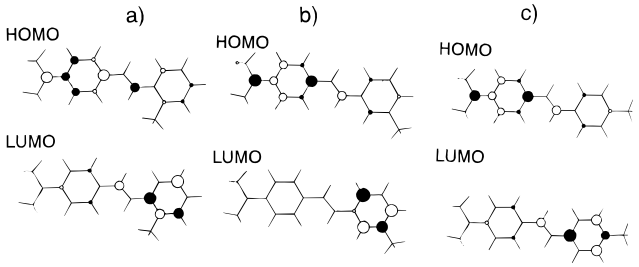

Figure 12. Frontier molecular orbitals (HOMO, LUMO) of the three DASPMI isomers for the planar conformation E: (a) ortho, (b) meta, and (c) para).

For the twisted conformations A_2, A_3, and P, the S_1 state consists of the virtually pure HOMO−LUMO transition which involves a maximum of charge translocation because HOMO and LUMO are localized on different fragments. The relevant orbitals for the different twisted conformations are shown in Figure 13a−c. One can see that for all single-bond twisted conformations, the HOMO is localized in that molecular part which bears the dimethylamino group, while the LUMO is localized in the other part of the twisted molecule. The reverse holds for the P conformation. This figure clearly shows that HOMO−LUMO excitation is connected with electron translocation, and it leads to a shift of the electron distribution in the molecule from the amino to the pyridinium end in the single-bond twisted conformations A_1, A_2, A_3 and in opposite direction for the P conformation.

In summary, the quantum chemical calculations demonstrate that TICT states connected with twisted single bonds are energetically low lying for the molecules investigated here. The following aspects are important:

For the conformations A_2 and A_3, the lowest TICT state is S_1; it is considerably lower than for conformation A_1.

While for the planar conformation the positive charge distribution extends over the whole molecule, the formation of the TICT states corresponds to localization of the positive charge on the twisted donor.

All three DASPMI isomers possess similar low lying TICT states.

The twisted double bond (P state) leads to a different charge distribution (positive charge localized on the pyridinium fragment in the excited state) and to relatively narrow S_1-S_0 energy gaps, especially for the meta-isomer.

To assess the possibility of spontaneous population of TICT (A_2, A_3) and P conformations on the S_1 hypersurface, information about the ground state hypersurface is also necessary in order to correct the energy gap results of Figure 11. We applied the semiempirical AM1 method to calculate the ground state surface. The results obtained are drawn in Figure 14. It can be seen that only the rotation of the double bond leads to a considerable ground state destabilization while the twisting of the three single bonds only affects the ground state energy negligibly (≈0.1 eV). Twisting of the dimethylamino group leads to a TICT state (A_1) possessing a higher energy than E*, P*, and the other two TICT states (A_2, A_3). This result signifies that a thermal population of the A_1 state is improbable while a population of the other two TICT states and of P* is probable because the energies are similar to that of the planar conformation E. The deactivation of the P* state should occur radiationless because of the small energy gap to the ground state. An emission from A_2 and A_3 states should be possible because the energies of the excited states are similar to that of the planar conformation. The TICT emission should be different from that of the conformation E because the fluorescence from a TICT state is forbidden at least in its limiting perpendicular conformation. Therefore, different effective fluorescence rate constants k_f are expected for conditions with varying proportions of TICT emission to the total spectrum. This was experimentally found as previously reported.[14]

Conclusions

This study demonstrates that both methods, the global analysis technique of wavelength dependent fluorescence decays and semiempirical quantum chemical calculations, are useful tools for the investigation of multiple fluorescence that occurs in several stilbazolium dyes. The method applied in this work consists of constructing the emission profiles of the different emitting species as described previously.[26] It is an alternative to a global target fit, which has been successfully applied in many other studies.[15−25] However, the global target technique requires rate constants that are usually evaluated by quenching procedures,[20] the isolation of only one emitting species, or using a reference compound.[25] Furthermore, an infinite number of

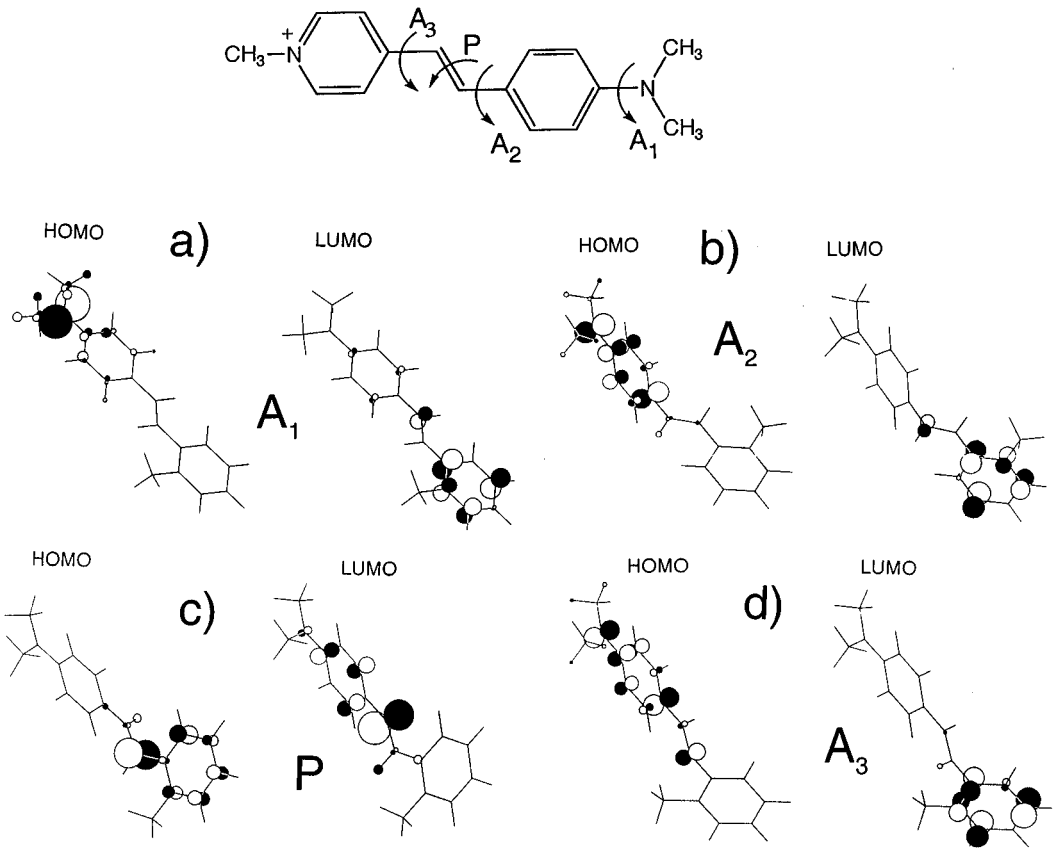

Figure 13. Relevant molecular orbitals for the different twisted conformations A_1 (a), A_2 (b), A_3 (d), and P* (c) for the case of the ortho-isomer. Qualitatively similar results were obtained for the para and meta-isomer.

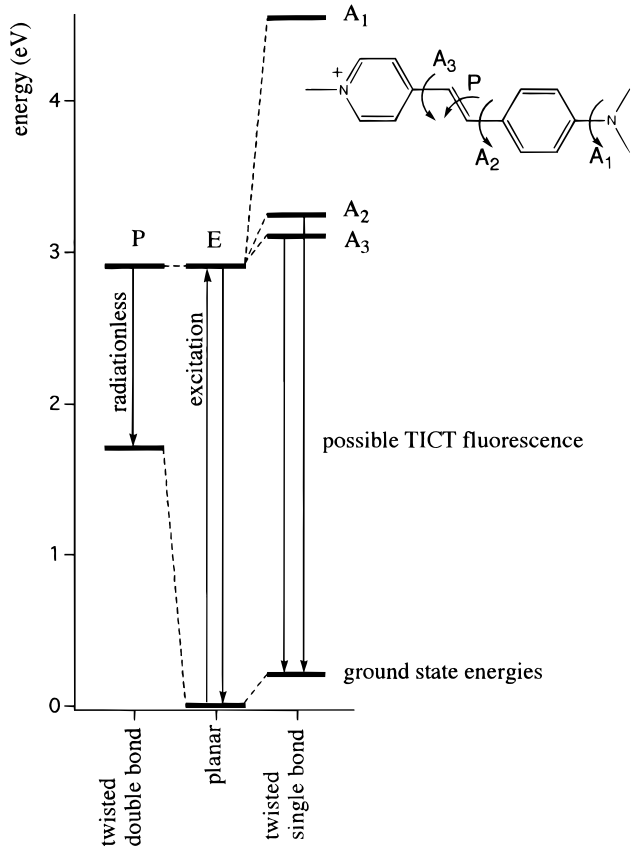

Figure 14. Calculated absolute energies of the different conformations of *p*-DASPMI by using the calculated ground state energies (AM1) in conjunction with the excitation energies.

solutions is obtained if reference data are not available. For this reason, we preferred the procedure described in this work because reference data are difficult to obtain for the molecules investigated here. The fluorescence properties of DASPMI (e.g. viscosity dependent fluorescence[14]) are important for many applications.[1,2] The quantum chemical calculations performed lead to the conclusion that these compounds are comparable with "disturbed cyanines".[27] Experimentally, they possess very low trans → cis isomerization quantum yields and therefore a high photostability. Investigations on compounds related to pyridine 1 support these considerations[45] and substantiate the occurrence of multiple fluorescence also for dyes with more than one olefinic double bond.

Acknowledgment. B.S. thanks gratefully the Alexander von Humboldt Foundation for a fellowship that gave the opportunity to carry out most of the lifetime measurements at the Technical University of Berlin. Additionally, the authors thank the former Bundesministerium für Forschung und Technologie, Project No. 055KTFAB9 for financial support. Prof. Bally, University of Fribourg/Switzerland, is gratefully acknowledged for the program MOPLOT.

Appendix

For the analysis of decay curves by global analysis, it is often useful to have analytical expressions for the DAS (decay associated spectra) as well as for the SAS (species associated spectra). The following procedure provides an easy way for the calculation of both. Furthermore, we demonstrate this for the consecutive and the parallel reaction mechanisms. In addition, extensions to more complicated schemes[44] can also easily derived in cases where the differential equation system can be solved for the photochemical mechanism proposed.

First, one needs to set up the differential equation systems for the reaction scheme considered.

(a) Consecutive Mechanism (A → B → C). With the assumption that back-reactions can be neglected, one obtains the following equations.

$$\frac{dA(t)}{dt} = -k_A^{c}A(t) \tag{A1}$$

$$\frac{dB(t)}{dt} = +k_4A(t) - k_B^{c}B(t) \tag{A2}$$

$$\frac{dC(t)}{dt} = +k_6B(t) - k_C^{c}C(t) \tag{A3}$$

$$A(0) = A_0 \tag{A4}$$

$$B(0) = 0 \tag{A5}$$

$$C(0) = 0 \tag{A6}$$

$$k_A^{C} = k_1 + k_4 \tag{A7}$$

$$k_B^{C} = k_2 + k_6 \tag{A8}$$

$$k_C^{C} = k_3 \tag{A9}$$

(b) Parallel Mechanism (C ← A → B). The following expressions are valid for this kind of reaction (no back-reactions).

$$\frac{dA(t)}{dt} = -k_A^{P}A(t) \tag{A10}$$

$$\frac{dB(t)}{dt} = +k_4A(t) - k_B^{P}B(t) \tag{A11}$$

$$\frac{dC(t)}{dt} = +k_8A(t) - k_C^{P}C(t) \tag{A12}$$

$$A(0) = A_0 \tag{A13}$$

$$B(0) = 0 \tag{A14}$$

$$C(0) = 0 \tag{A15}$$

$$k_A^{P} = k_1 + k_4 + k_8 \tag{A16}$$

$$k_B^{P} = k_2 \tag{A17}$$

$$k_C^{P} = k_3 \tag{A18}$$

The solutions of the differential equation system for both mechanisms can be expressed in the general form of eqs A19−A21. The consideration of spectra instead of the time dependent decay of the excited state at only one wavelength makes it necessary to multiply each time dependent population $X(t)$ by a specific spectral contour $x(\lambda)$ that is characteristic for each species X (X = A, B, and C, respectively). The spectral contours are defined through eq 5. They stand in relation with the emission from the species X because integration of the spectral contours over the wavelength yields the radiative rate constant of the species X.

$$A(t,\lambda) = a(\lambda)[a_1 \exp(-\theta_1 t)] \tag{A19}$$

$$B(t,\lambda) = b(\lambda)[b_1 \exp(-\theta_1 t) + b_2 \exp(-\theta_2 t) + b_3 \exp(-\theta_3 t)] \tag{A20}$$

$$C(t,\lambda) = c(\lambda)[c_1 \exp(-\theta_1 t) + c_2 \exp(-\theta_2 t) + c_3 \exp(-\theta_3 t)] \tag{A21}$$

For calculating of SAS, one has to integrate each equation in eqs A19−A21 over time, which leads to the following equation system A22−A24:

$$\mathrm{SAS_A}(\lambda) = a(\lambda)\left[\frac{a_1}{\theta_1}\right] \tag{A22}$$

$$\mathrm{SAS_B}(\lambda) = b(\lambda)\left[\frac{b_1}{\theta_1} + \frac{b_2}{\theta_2} + \frac{b_3}{\theta_3}\right] \tag{A23}$$

$$\mathrm{SAS_C}(\lambda) = c(\lambda)\left[\frac{c_1}{\theta_1} + \frac{c_2}{\theta_2} + \frac{c_3}{\theta_3}\right] \tag{A24}$$

The DAS values are calculated from eqs A19−A21 by adding up each coefficient of the exponential terms vertically:

$$\mathrm{DAS_1}(\lambda) = a_1a(\lambda) + b_1b(\lambda) + c_1c(\lambda) \tag{A25}$$

$$\mathrm{DAS_2}(\lambda) = +b_2b(\lambda) + c_2c(\lambda) \tag{A26}$$

$$\mathrm{DAS_3}(\lambda) = +b_3b(\lambda) + c_3c(\lambda) \tag{A27}$$

The problem is to calculate the spectral contours $a(\lambda)$, $b(\lambda)$, and $c(\lambda)$, which are still unknown. Equations A25−A27 are a linear inhomogeneous equation system for $a(\lambda)$, $b(\lambda)$, and $c(\lambda)$. On the other hand, the DAS-values are known from the experiment through eq 1. Therefore, mathematical expressions for $a(\lambda)$, $b(\lambda)$, and $c(\lambda)$ can be derived from eqs A25−A27. The next step is to introduce expressions obtained for the spectral contours in eqs A22−A24. One can see that the SAS values are linear combinations of the DAS values, and SAS data are proportional to their spectral profiles.

References and Notes

(1) Spooner, S. P.; Whitten, D. G. Photoreactions in Monolayer Films and Langmuir-Blodgett Assemblies. In *Photochemistry in Organized & Constrained Media*; Ramamurthy, V., Ed.; VCH Publishers Inc.: Weinheim, 1991; Chapter 15, pp 691−739.

(2) Ulmann, A. In *An Introduction to Ultrathin Organic Films-From Langmuir Blodgett to Self Assembly*; Academic Press: San Diego, CA, 1991; Chapters 3 and 5.

(3) Strehmel, B.; Strehmel, V.; Younes, M.; Wartewig, S. *Progress Colloid Polym. Sci.* **1992**, *90*, 83.

(4) Ephardt, H.; Fromherz, P. *J. Phys. Chem.* **1989**, *93*, 7717.

(5) Görner, H.; Gruen, H. *J. Photochem.* **1985**, *28*, 329.

(6) Bringmann, D.; Ernsting, N. P. *J. Chem. Phys.* **1995**, *102*, 2691.

(7) Fromherz, P.; Dambacher, K. H.; Ephardt, H.; Lambacher, A.; Müller, C. O.; Neigl, R.; Schaden, H.; Schenk, O.; Vetter, T. *Ber. Bunsen-Ges. Phys. Chem.* **1991**, *95*, 1333.

(8) Loew, L. M.; Scully, S.; Simpson, L.; Waggoner, A. S. *Nature* **1979**, *281*, 497.

(9) Ephardt, H.; Fromherz, P. *J. Phys. Chem.* **1991**, *95*, 6792.

(10) Fromherz, P.; Heilemann, A. *J. Phys. Chem.* **1992**, *96*, 6964.

(11) Grabowski, Z. R.; Rotkiewicz, K.; Siemiarczuk, A.; Cowley, D. J.; Baumann, W. *Nouv. J. Chim.* **1979**, *3*, 443.

(12) Rettig, W. *Angew. Chem., Int. Ed. Engl.* **1986**, *25*, 971.

(13) W. Rettig, In *Photoinduced Electron Transfer*; Mattay, J., Ed.; Topics in Current Chemistry; Springer Verlag: Berlin, 1994; pp 93−141.

(14) Strehmel, B.; Rettig, W. *J. Biomed. Opt.* **1996**, *1*, 98.

(15) Zachariasse, K. A.; Striker, G. *Chem. Phys. Lett.* **1988**, *145*, 251.

(16) Snare, M. J.; Thistlethwaite, P. J.; Ghiggino, K. P. *J. Am. Chem. Soc.* **1983**, *105*, 3328.

(17) Andriessen, R.; Boens, N.; De Schryver, F. C. *J. Phys. Chem.* **1991**, *95*, 2047.

(18) Amelot, M.; Andriessen, R.; Van den Bergh, V.; De Schryver, F. C. *J. Phys. Chem.* **1991**, *95*, 2041.
(19) Van Dommelen, L.; Amelot, M.; De Schryver, F. C.; Kowalczyk, A. *J. Phys. Chem.* **1993**, *97*, 11738.
(20) Khalil, M. M. H.; Boens, N.; Van der Auerwaer, M.; Amelot, M.; Andriessen, R.; Hofkens, J.; De Schryver, F. C. *J. Phys. Chem.* **1991**, *95*, 9375.
(21) Leinhos, U.; Kühnle, U.; Zachariasse, K. A. *J. Phys. Chem.* **1991**, *95*, 2013.
(22) Davenport, L.; Knutson, J. R.; Brand, L. *Biochemistry* **1986**, *25*, 1186.
(23) Beechem, J. M.; Amelot, M.; Brand, L. *Chem. Phys. Lett.* **1985**, *120*, 460.
(24) Knutson, J. R.; Beechem, J. M.; Brand, L. *Chem. Phys. Lett.* **1983**, *102*, 501.
(25) Beechem, J. M.; Gratton, E.; Amelot, M.; Knutson, J. R.; Brand, L. In *Topics in Advanced Fluorescence Spectroscopy*; Lakowicz, J. R., Ed.; Plenum Press: New York, 1991; Vol. 2, p 241.
(26) (a) Löfroth, J.-E. *J. Phys. Chem.* **1986**, *90*, 1160. (b) Löfroth, J.-E. *Anal. Instrum.* **1985**, *14*, 403.
(27) Rettig, W.; Strehmel, B.; Majenz, W. *Chem. Phys.* **1993**, *173*, 525.
(28) Heinze, J; Kopf, U. *Anal. Chem.* **1984**, *56*, 1931.
(29) (a) Rettig, W.; Vogel, M.; Klock, A. *EPA Newsl.* **1986**, *27*, 41. (b) Vogel, M.; Rettig, W. *Ber. Bunsen-Ges. Phys. Chem.* **1987**, *91*, 1241.
(30) O'Connor, D. V.; Phillips, D. *Time-correlated Single Photon Counting*; Academic Press: London, 1984.
(31) Globals Unlimited, commercially available from the University of Illinois, 1992.
(32) Del Bene, J.; Jaffé, H. H. *J. Chem. Phys.* **1968**, *48*, 1807.
(33) Del Bene, J.; Jaffé, H. H. *J. Chem. Phys.* **1968**, *48*, 4050.
(34) Sutton, L. E. *Tables and Interatomic Distances and Configurations in Molecules*; The Chemical Society: London, 1965.
(35) Rettig, W.; Bonačić-Koutecký, V. *Chem. Phys. Lett.* **1979**, *62*, 115.
(36) Albrecht, B.; Matzinger, S.; Bally, T. Version of MOPLOT for DOS PCs (available from Prof. Bally, University of Fribourg, Switzerland, upon request).
(37) Van Dommelen, L.; Boens, N.; Amelot, M.; De Schryver, F. C.; Kowalczyk, A. *J. Phys. Chem.* **1993**, *97*, 11753.
(38) Lapouyade, R.; Czeschka, K.; Majenz, W.; Rettig, W. *Chem. Phys. Lett.* **1992**, *96*, 9643.
(39) Lapouyade, R.; Kuhn, A.; Létard, J. F.; Rettig, W. *Chem. Phys. Lett.* **1993**, *208*, 48.
(40) Rettig, W. In *Modern Models of Bonding and Delocalization, Molecular Structure and Energetics, Vol. 6*; Liebman, J., Greenberg, A., Eds.; VCH Publishers: New York, 1988; p 229.
(41) Letard, J. F.; Lapouyade, R.; Rettig, W. *Chem. Phys.* **1994**, *186*, 119.
(42) Orlandi, G.; Siebrand, W. *Chem. Phys. Lett.* **1975**, 30, 352.
(43) Michl, J.; Bonačić-Koutecký, V. *Electronic Aspects of Organic Photochemistry*; John Wiley & Sons: New York, Chichester, Brisbane, Toronto, Singapore, 1990.
(44) Information about solutions of differential equations, SAS and DAS equations, and other parameters for more complicated reaction schemes are available from the authors upon request.
(45) Strehmel, B; Rettig, W. *BESSY Ann. Rep.* **1993**, 170.